Dalton Transactions

RSC Publishing

PAPER

View Article Online
View Journal | View Issue

Cite this: *Dalton Trans.*, 2013, **42**, 3876

The synthesis, structures and magnetic properties of polynuclear Ru^{III}–3d (3d = $Mn^{II/III}$, Ni^{II}, Cu^{II}) compounds based on $[Ru^{III}(Q)_2(CN)_2]^{-}$†

Jing Xiang,[a,b] Li-Hui Jia,[c] Bing-Wu Wang,[c] Shek-Man Yiu,[a] Shie-Ming Peng,[d] Wai-Yeung Wong,[e] Song Gao*[c] and Tai-Chu Lau*[a]

Received 3rd October 2012,
Accepted 10th December 2012

DOI: 10.1039/c2dt32331a

www.rsc.org/dalton

The synthesis, crystal structures and magnetic properties of six cyano-bridged heterobimetallic compounds prepared from a paramagnetic Ru^{III} building block, *trans*-$(PPh_4)[Ru^{III}(Q)_2(CN)_2]$ (**1**) (Q = the anion of 8-hydroxyquinoline), are described. **1** reacts with hydrated $MnCl_2$ in MeOH or DMF to produce a trinuclear compound $\{[Ru^{III}(Q)_2(CN)_2]_2[Mn^{II}(MeOH)_4]\}\cdot 8MeOH$ (**2**), or a 1-D *zigzag* chain $\{[Mn^{II}(DMF)_2(Cl)](\mu\text{-}CN)_2[Ru^{III}(Q)_2]\}_n$ **(3)**. The Mn^{II} has a distorted octahedral environment in **2** and a trigonal-bipyramidal environment in **3**. **1** reacts with $[Mn^{III}(L^1)(Cl)(H_2O)]$ in MeOH to produce the 1-D $\{[Ru^{III}(Q)_2](\mu\text{-}CN)_2[Mn^{III}(L^1)]\}_n$ (**4**) that consists of alternating Mn^{III} and Ru^{III} units. **1** also reacts with $[Cu^{II}(cyclam)Br_2]$ and $[Ni^{II}(cyclam)Cl_2]$ in MeOH to produce the trinuclear complexes $[Ru^{III}(Q)_2(CN_2)]_2[M^{II}(cyclam)]$ (M = Cu^{II} (**5**) and Ni^{II} (**6**)). On the other hand, the reaction of **1** with $[Ni^{II}(cyclen)Cl_2]$ produces a 1-D *zigzag* chain $\{([Ru^{III}(Q)_2(CN_2)][Ni^{II}(cyclen)])[Ru^{III}(Q)_2(CN_2)]\}_n$ (**7**). Compounds **2–4** exhibit antiferromagnetic coupling between Ru^{III} and $Mn^{III/II}$ centres. Antiferromagnetic coupling also occurs between Ru^{III} and Cu^{II} centres in **5**. On the other hand, compounds **6** and **7** exhibit ferromagnetic coupling between Ru^{III} and Ni^{II} through cyanide bridges.

Introduction

The use of paramagnetic cyanometallates as building blocks for the construction of polynuclear compounds has attracted much attention in recent years, because these materials may possess interesting and potentially useful magnetic properties.[1,2] A variety of 3d cyanometallates have been known for decades, but recently 4d and 5d cyanometallates have also been reported, such as *trans*-$[Re^{IV}Cl_4(CN)_2]^{2-}$,[3] $Mo^{III}(Me_3tacn)(CN)_3$,[4] *fac*-$[Re^{II}(triphos)(CN)_3]^{-}$,[5] $(Me_3tacn)Mo^{III}(CN)_4]^{-}$,[6] $[Mo^{I}(CN)_5(NO)]^{2-}$,[7] $[Mo^{III}(CN)_6]^{3-}$,[8] $[W^{IV/V}(bipy)(CN)_6]^{2-/-}$,[9] $[Mo^{III}(CN)_7]^{4-}$,[10] $[Re^{IV}(CN)_7]^{3-}$,[11] $[M^{IV/V}(CN)_8]^{4-/3-}$ (M = Mo, W),[12] and $[Nb^{III/IV}(CN)_8]^{5-/4-}$.[13] We have been interested in the design of paramagnetic Ru and Os building blocks because Ru and Os form stable complexes with a variety of ligands and in various oxidation states. Hence it is anticipated that polynuclear compounds with novel magnetic properties may be prepared by using Ru and Os building blocks. We have reported the synthesis of a number of cyanoruthenium(III) and osmium(III) complexes, including $[M^{III}(salen)(CN)_2]^{-}$ (M = Ru, Os), *trans*-$[Ru^{III}(acac)_2(CN)_2]^{-}$ and *mer*-$[Ru^{III}(CN\text{-}sap)(CN)_3]^{2-}$. These cyano complexes have been used to construct a series of 3d–Ru^{III}/Os^{III} and 4f–Ru^{III} polynuclear compounds that exhibit a wide variety of magnetic properties.[14] We have also recently designed a new cyanoruthenium(III) building block, $(PPh_4)[Ru^{III}(Q)_2(CN)_2]$ (**1**, Q = the anion of 8-hydroxyquinoline,

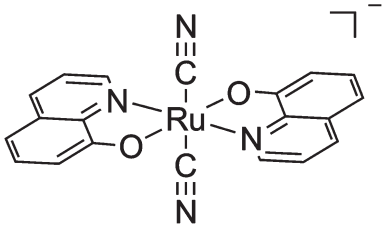

Fig. 1 Structure of the anion of **1**.

[a]*Department of Biology and Chemistry, Institute of Molecular Functional Materials, City University of Hong Kong, Tat Chee Avenue, Kowloon Tong, Hong Kong, China. E-mail: bhtclau@cityu.edu.hk; Fax: (+852)34420522*
[b]*College of Chemistry and Environmental Engineering, Yangtze University, Jingzhou 434020, HuBei, PR China*
[c]*State Key Laboratory of Rare Earth Materials Chemistry and Applications and PKU-HKU Joint Laboratory on Rare Earth Materials and Bioinorganic Chemistry, Peking University, Beijing 100871, China. E-mail: gaosong@pku.edu.cn; Fax: (+86) 10-62751708*
[d]*Department of Chemistry, National Taiwan University, Taipei 106, Taiwan*
[e]*Department of Chemistry, Hong Kong Baptist University, Waterloo Road, Kowloon Tong, Hong Kong, China*

†Electronic supplementary information (ESI) available. CCDC 903912–903917. For ESI and crystallographic data in CIF or other electronic format see DOI: 10.1039/c2dt32331a

Fig. 1).[15] We anticipate that π–π interactions between the quinolinolato ligands could provide additional attractive forces for the construction of supramolecular structures with possibly enhanced magnetic interactions between paramagnetic metal centres. Indeed, we have prepared a trinuclear complex, $\{[Ru^{III}(Q)_2(CN)]_2(\mu\text{-}CN)_2[Co^{II}(MeOH)_4]\}\cdot 8MeOH$, that exhibits 3-D long range ferromagnetic ordering below 4.5 K. In this compound, π–π interactions connect the discrete trinuclear units into an extended 3-D network that results in the observed magnetic behaviour. Herein, we report the synthesis and magnetic properties of a series of 3d/Ru^{III} (3d = $Mn^{II/III}$, Ni^{II}, Cu^{II}) polynuclear compounds constructed from this new building block. We demonstrate again that π–π interactions between the quinolinolato ligands play a crucial role in determining the structure and magnetic properties of these polynuclear compounds.

Experimental section

Materials and physical measurements

$(PPh_4)[Ru^{III}(Q)_2(CN)_2]$ (**1**) was prepared by a literature procedure.[15] The Schiff base ligand *N*,*N*′-bis(salicylidene)-*o*-cyclohexylenediamine (H_2L^1) was synthesized by condensation of salicylaldehyde with the corresponding diamine in refluxing ethanol. 1,4,8,11-Tetraazacyclotetradecane (cyclam), 1,4,7,10-tetraazacyclododecane (cyclen) and 8-hydroxyquinoline (HQ) were purchased from Aldrich Chemical Co. and used without further purification. IR spectra were obtained as KBr discs using a Nicolet 360 FT-IR spectrophotometer. Elemental analysis was performed using an Elementar Vario EL Analyzer. Variable-temperature magnetic susceptibility, ac magnetic susceptibility, and field dependence of magnetization were measured on a Quantum Design MPMS XL-5 SQUID system. Background corrections were done by experimental measurement on the sample holder. The experimental susceptibilities were corrected for the diamagnetism of the constituent atoms (Pascal's tables).

X-ray crystallography

Crystals suitable for X-ray diffraction analysis were obtained for compounds **2–7**. Crystal data and experimental details are given in Table 1. X-ray diffraction data were collected at 100 K on an Oxford CCD or a NONIUS Kappa CCD diffractometer using graphite-monochromated Mo Kα radiation (λ = 0.71073 Å) for **2–5** and Cu Kα (λ = 1.54178 Å) for **6** and **7** in the ω-scan mode. Absorption corrections were done by the multi-scan method. The structures were resolved by the heavy-atom Patterson method or direct methods and refined by full-matrix least-squares using SHELX-97 and expanded using Fourier techniques.[16,17] All non-hydrogen atoms were refined anisotropically. H atoms were generated by the program SHELXL-97.[18] The positions of H atoms were calculated on the basis of riding mode with thermal parameters equal to 1.2 times that of the associated C atoms, and participated in the calculation of final *R*-indices. CCDC for **2–7**: 903912–903917.

Table 1 Crystal and structural refinement data for compounds **2–7**

Compounds	**2**·8MeOH	**3**	**4**·2MeOH	**5**·4MeOH	**6**·4MeOH	**7**·3MeOH
Formula	$C_{52}H_{72}MnN_8O_{16}Ru_2$	$C_{26}H_{26}ClMnN_6O_4Ru$	$C_{42}H_{40}MnN_6O_6Ru$	$C_{54}H_{60}N_{12}CuO_8Ru_2$	$C_{54}H_{60}N_{12}NiO_8Ru_2$	$C_{51}H_{52}N_{12}NiO_7Ru_2$
M_r	1322.26	677.99	880.81	1270.84	1265.99	1205.90
Cryst syst	Monoclinic	Monoclinic	Triclinic	Monoclinic	Monoclinic	Triclinic
Space group	$P2_1/c$	$C2/c$	$P\bar{1}$	$P2_1/n$	$P2_1/n$	$P\bar{1}$
a/Å	8.8446(2)	14.5641(4)	12.568(4)	8.9277(12)	8.9374(3)	11.7692(4)
b/Å	12.6986(3)	10.4098(3)	13.049(4)	20.948(3)	20.4558(10)	13.5116(4)
c/Å	27.9148(7)	18.0972(5)	13.520(3)	15.023(2)	15.3293(7)	17.1714(6)
α	/	/	82.23(2)	/	/	95.113(2)
β	92.1090(11)	92.669(3)	74.24(2)	104.175(2)	104.278(2)	96.982(2)
γ	/	/	63.88(3)	/	/	102.153(2)
V/Å^3	3133.10(13)	2740.72(13)	1915.5(9)	2723.9(6)	2716.0(2)	2631.04(15)
Z	2	4	2	2	2	2
ρ_{calcd}/mg m^{-3}	1.402	1.643	1.527	1.530	1.548	1.522
F(000)	1362	1368	902	1266	1296	1228
Collected refl.	5498	2446	7382	4741	6160	11 896
Unique reflns	4127	2382	2118	3218	4348	7215
Final R indices, $I > 2\sigma(I)$ R	0.1059(0.2858)	0.0217(0.0453)	0.0852(0.2324)	0.0701(0.1046)	0.0501(0.0825)	0.0552(0.1041)
GOF	1.185	1.057	0.751	1.069	1.053	1.024
No. of parameters	326	181	434	349	458	649

Synthesis

{[$Ru^{III}(Q)_2(CN)]_2(\mu\text{-}CN)_2[Mn^{II}(MeOH)_4]$} (2). A solution of $(PPh_4)[Ru^{III}(Q)_2(CN)_2]$ (**1**) (50 mg, 0.064 mmol) in methanol (5 mL) and a solution of $MnCl_2{\cdot}4H_2O$ (19.8 mg, 0.10 mmol) in methanol (5 mL) were placed in each arm of a H-tube. Methanol (*ca.* 40 mL) was slowly added to the tube until the two arms were able to mix. Dark red block-shaped crystals suitable for X-ray crystallography were obtained after standing the solution for 2 weeks. Yield: 52%. Elemental analysis (%) calcd for $C_{44}H_{40}MnN_8O_8Ru_2{\cdot}H_2O$: C, 48.76; H, 3.91; N, 10.34. Found: C, 48.56; H, 4.04; N, 10.02. IR (KBr)/cm^{-1}: ν(C≡N) 2124, 2103.

{[$Mn^{II}(DMF)_2(Cl)](\mu\text{-}CN)_2[Ru^{III}(Q)_2]$}$_n$ (3). A solution of **1** (50 mg, 0.064 mmol) in DMF (5 mL) and a solution of $MnCl_2{\cdot}4H_2O$ (19.8 mg, 0.10 mmol) in DMF (5 mL) were placed in each arm of a H-tube. DMF (*ca.* 15 mL) was slowly added to the tube until the two arms were able to mix. Dark red block-shaped crystals suitable for X-ray crystallography were obtained after standing the solution for 2 weeks. Yield: 54%. Elemental analysis (%) calcd for $C_{26}H_{26}ClMnN_6O_4Ru$: C, 46.06; H, 3.87; N, 12.40. Found: C, 46.10; H, 3.95; N, 12.19. IR (KBr)/cm^{-1}: ν(C≡N) 2126, 2108.

{[$Ru^{III}(Q)_2](\mu\text{-}CN)_2[Mn^{III}(L^1)]$}$_n$ (4). A solution of **1** (50 mg, 0.064 mmol) in DMF–MeOH (5 mL, 1 : 1, v/v) and a solution of $[Mn^{III}(L^1)(Cl)(H_2O)]$ (28 mg, 0.064 mmol) in DMF–MeOH (5 mL) were placed in each arm of a H-tube. DMF–MeOH (*ca.* 15 mL) was slowly added to the tube until the two arms were able to mix. Dark red block crystals suitable for X-ray crystallography were obtained after standing the solution for 2 weeks. Yield: 40%. Anal. calcd (found) for $C_{40}H_{32}MnN_6O_4Ru{\cdot}3H_2O$: C, 55.17 (55.33); H, 4.40 (4.23); N, 9.65 (9.80). IR: (KBr)/cm^{-1}: ν(C≡N) 2107.

{[$Ru^{III}(Q)_2(CN)]_2(\mu\text{-}CN)_2[Cu^{II}(cyclam)]$} (5). A solution of **1** (50 mg, 0.064 mmol) in methanol (5 mL) and a solution of $[Cu^{II}(cyclam)Br_2]$ (42 mg, 0.10 mmol) in methanol (5 mL) were placed in each arm of a H-tube. Methanol (*ca.* 40 mL) was slowly added to the tube to cover the two arms. Dark red block-shaped crystals suitable for X-ray crystallography were obtained after standing the solution for 2 weeks at room temperature. Yield: 76%. Anal. calcd (found) for $C_{50}H_{48}CuN_{12}O_4Ru_2{\cdot}2H_2O$: C, 50.78 (50.52); H, 4.43 (4.67); N, 14.21 (14.11). IR (KBr)/cm^{-1}: ν(C≡N) 2100.

{[$Ru^{III}(Q)_2(CN)]_2(\mu\text{-}CN)_2[Ni^{II}(cyclam)]$} (6). A solution of **1** (50 mg, 0.064 mmol) in methanol (5 mL) and a solution of $[Ni^{II}(cyclam)Cl_2]$ (20 mg, 0.10 mmol) in methanol (5 mL) were placed in each arm of a H-tube. Methanol (*ca.* 40 mL) was slowly added to the tube until the two arms were able to mix. Dark red block-shaped crystals suitable for X-ray crystallography were obtained after standing the solution for 2 weeks. Yield: 80%. Anal. calcd (found) for $C_{50}H_{44}NiN_{12}O_2Ru_2{\cdot}2H_2O$: C, 50.99 (50.67); H, 4.45 (4.71); N, 14.27 (14.30). IR (KBr)/cm^{-1}: ν (C≡N) 2106.

{[$Ru^{III}(Q)_2](\mu\text{-}CN)_2[Ni^{II}(cyclen)]$}$_n$[$Ru^{III}(Q)_2(CN)_2$]$_n$ (7). A solution of **1** (50 mg, 0.064 mmol) in methanol (5 mL) and a solution of $[Ni^{II}(cyclen)Cl_2]$ (30 mg, 0.10 mmol) in methanol (5 mL) were placed in each arm of a H-tube. Methanol (*ca.* 40 mL) was slowly added to the tube until two arms were able to mix. Dark red block-shaped crystals suitable for X-ray crystallography were obtained after standing the solution for 2 weeks. Yield: 54%. Anal. calcd (found) for $C_{48}H_{44}N_{12}NiO_4Ru_2{\cdot}2H_2O$: C, 50.14 (49.98); H, 4.21 (4.45); N, 14.62 (14.37). IR (KBr)/cm^{-1}: ν(C≡N) 2126, 2099.

Results and discussion

The reaction of **1** with hydrated $MnCl_2$ in MeOH or DMF produced **2** and **3** as dark brown crystals, respectively (Scheme 1). The IR shows two ν(C≡N) stretches at 2124 and 2103 cm^{-1} in **2** and 2126 and 2108 cm^{-1} in **3** that are at higher frequencies than those in **1** (2095 cm^{-1}).[15]

The structure of **2** has been determined by X-ray crystallography. Selected bond lengths (Å) and bond angles (°) are summarized in Table 2. It is a trinuclear complex that crystallizes in a $P2_1/c$ group system with an inversion center on Mn^{II}. The Mn^{II} is octahedrally coordinated by two $[Ru^{III}(Q)_2(CN)_2]^-$ units through the nitrogen atoms in a *trans* configuration, and four methanol molecules occupy the basal plane (Fig. 2). The structure is similar to the reported complex {$[Co^{II}(CH_3OH)_4]$-$[Ru^{III}(Q)_2(CN)_2]_2$}·8MeOH.[15] The bond lengths and bond angles in the $[Ru(Q)_2(CN)_2]^-$ unit are essentially identical to those of **1**, indicating that the oxidation state of the ruthenium centre is retained. There is extensive face-to-face π–π stacking among the quinolinolato ligands (centroid-to-centroid distance = 3.698 Å) which connects the discrete molecules into 1-D supramolecular double chains, as shown in Fig. 3. The closest intermolecular Ru···Ru separation along the *a*-axis is 8.845 Å in **2** and the closest intramolecular Mn···Ru distance is 5.311 Å.

The crystal structure of **3** is shown in Fig. 4. It is a 1-D *zigzag* chain consisting of alternating $[Ru^{III}(Q)_2(CN)_2]^-$ and Mn^{II} moieties linked together by the CN^- ligands. Selected bond lengths (Å) and bond angles (°) are listed in Table 3. The Mn^{II} in **3** has a distorted trigonal bipyramidal geometry (τ = 0.860)[19] and is coordinated by two DMF, two nitrogen atoms from bridging CN^- ligands and an apical Cl^- ligand. The inter-chain Mn···Ru and Ru···Ru separations are 5.360 Å and 9.049 Å, respectively. The closest Ru···Ru distance is 8.951 Å. As in **2**, there is extensive inter-chain π–π stacking among the quinolinolato ligands (centroid-to-centroid distance = 3.727 Å) along the *a*-axis, resulting in a 3-D supramolecular structure (Fig. 5).

The reaction of **1** with $[Mn^{III}(L^1)(Cl)(H_2O)]$ in DMF–MeOH affords a 1-D chain (**4**). The IR spectrum of **4** shows a ν(C≡N) stretch at 2107 cm^{-1}, which is at a higher frequency than that of **1**. The crystal structure of **4** has been determined by X-ray crystallography (Fig. 6, Table 4). It consists of alternating *trans*-$Ru^{III}(Q)_2$ and $Mn^{III}L^1$ units bridged by cyanide ligands. This structure is similar to the reported Ru^{III}–Mn^{III} complex $[Ru^{III}$-$(salen)(CN)_2][Mn^{III}(L)]$ (L = *N*,*N*′-(1-methylethylene)bis(2-hydroxynaphthalene-1-carbaldehydeneiminate)dianion).[20] Each Mn^{III} ion has a Jahn–Teller distorted octahedral geometry. The equatorial Mn–N and Mn–O distances (1.881(8)–1.989(9) Å) are much

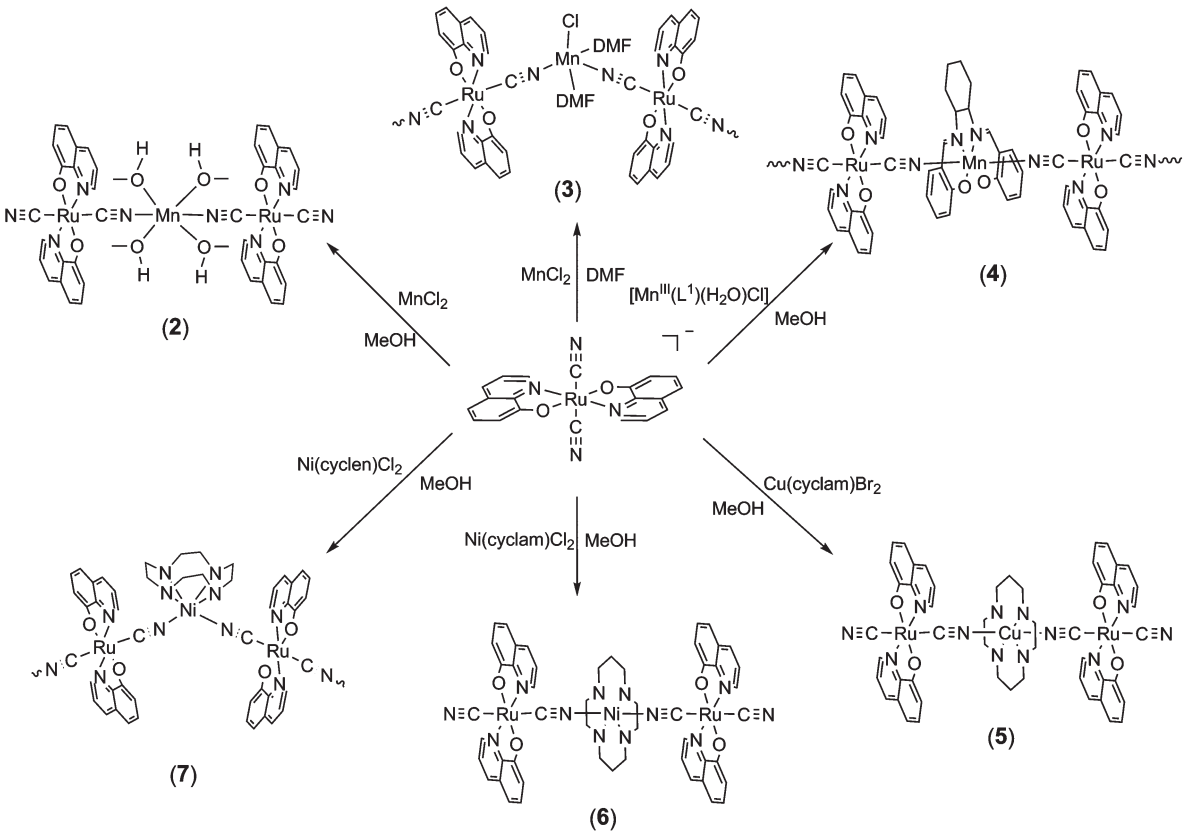

Scheme 1 Reactions of **1** with 3d paramagnetic centers.

Table 2 Selected geometric parameters (Å, °) for **2**

Ru–O1	1.924 (10)	Ru–N3	2.097 (11)
Ru–N4	2.058 (12)	Mn–N1	2.156 (9)
Ru–C1	2.060 (10)	Mn–O4	2.177 (13)
Ru–O2	2.066 (10)	Mn–O3	2.238 (13)
Ru–C2	2.069 (10)	N1–Mn–O4	86.6 (4)
O1–Ru–N4	102.7 (5)	N1–Mn–O4^{i}	93.4 (4)
O1–Ru–C1	88.1 (5)	N4–Ru–N3	175.2 (4)
N4–Ru–C1	86.6 (4)	C1–Ru–N3	93.3 (4)
O1–Ru–O2	175.9 (4)	O2–Ru–N3	95.6 (4)
N4–Ru–O2	79.6 (4)	C2–Ru–N3	88.1 (4)
C1–Ru–O2	88.7 (5)	N1–Mn–O3^{i}	91.9 (4)
O1–Ru–C2	91.1 (4)	N1–Mn–O3	88.1 (4)
N4–Ru–C2	92.2 (4)	O1–Ru–N3	82.1 (4)
C1–Ru–C2	178.3 (5)	O4–Mn–O3	85.4 (5)
O2–Ru–C2	92.2 (4)	O4^{i}–Mn–O3	94.6 (5)

Symmetry code: (i) $-x$, $-y+1$, $-z$.

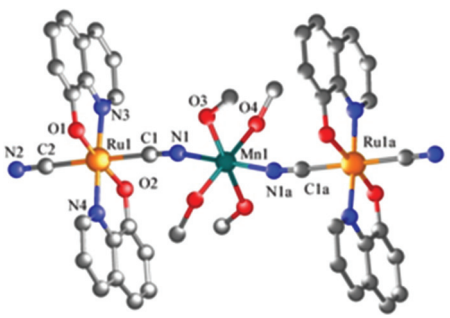

Fig. 2 The perspective view of **2** (symmetry code: (a) $+x$, $0.5-y$, $0.5+z$).

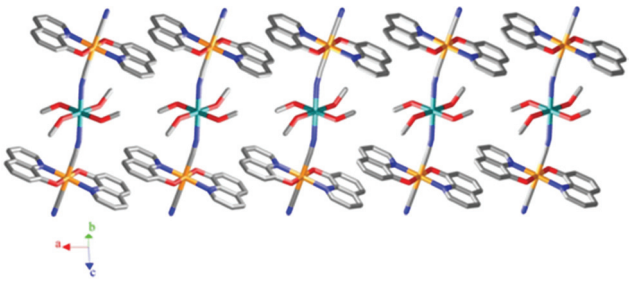

Fig. 3 Packing diagram of **2** showing π–π stacking interactions between the quinolinolato rings.

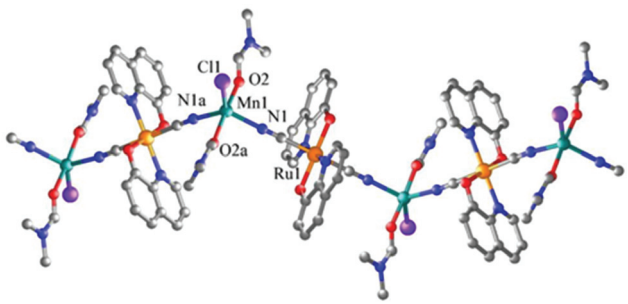

Fig. 4 The perspective view of **3** (symmetry code: (a) $-x+2$, $-y+2$, $-z+2$).

shorter than the axial Mn–N and Mn–O distances (2.286(10)–2.302(10) Å). The closest intrachain Ru···Mn separation is

Table 3 Selected geometric parameters (Å, °) for **3**

Ru1–O1	2.005 (2)	Mn1–O2	2.155 (2)
Ru1–N2	2.076 (3)	Mn1–N1	2.157 (3)
Ru1–C1	2.084 (3)	Mn1–Cl1	2.3821 (13)
$N2^{i}$–Ru1–C1	89.17 (12)	N1–Mn1–Cl1	119.70 (8)
O1–Ru1–N2	81.06 (11)	C1–N1–Mn1	173.8 (3)
$O1^{i}$–Ru1–N2	98.94 (11)	O2–Mn1–$O2^{ii}$	172.24 (14)
O1–Ru1–C1	90.88 (11)	O2–Mn1–N1	84.98 (10)
$O1^{i}$–Ru1–C1	89.12 (11)	$O2^{ii}$–Mn1–N1	91.17 (10)
N2–Ru1–C1	90.83 (12)	N1–Mn1–$N1^{ii}$	120.60 (16)
O2–Mn1–Cl1	93.88 (7)		

Symmetry code: (i) $-x + 2, -y + 2, -z + 2$; (ii) $-x + 2, y, -z + 3/2$.

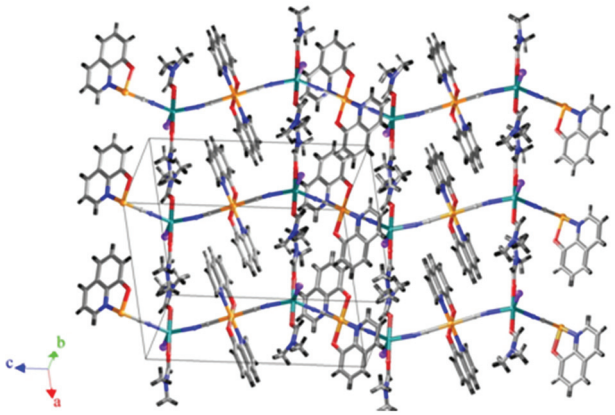

Fig. 5 Packing diagram of **3** showing the π–π interactions.

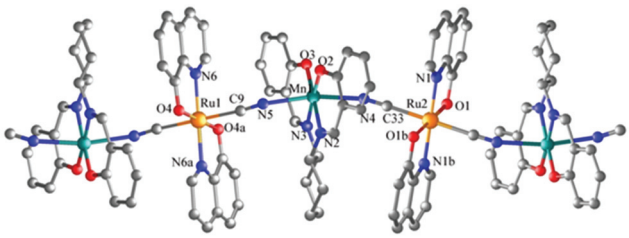

Fig. 6 The perspective view of **4** (symmetry codes: (a) $-x + 1, -y, -z + 1$ (b) $-x, -y, -z$).

Table 4 Selected bond lengths (Å) and bond angles (°) of **4**

Ru1–O4	1.927 (9)	Mn1–O2	1.881 (8)
Ru1–C9	2.064 (12)	Mn1–O3	1.885 (7)
Ru1–N6	2.080 (13)	Mn1–N3	1.971 (10)
Mn1–N4	2.286 (10)	Mn1–N2	1.989 (9)
Mn1–N5	2.302 (10)		
$O4^{i}$–Ru1–C9	87.5 (4)	N2–Mn1–N4	83.7 (4)
O4–Ru1–C9	92.5 (4)	O2–Mn1–O3	92.3 (3)
O4–Ru1–$N6^{i}$	82.0 (5)	O2–Mn1–N3	175.9 (4)
C9–Ru1–$N6^{i}$	84.9 (4)	O3–Mn1–N3	91.8 (4)
O4–Ru1–N6	98.0 (5)	O2–Mn1–N2	92.8 (4)
C9–Ru1–N6	95.1 (4)	O3–Mn1–N2	174.8 (4)
O2–Mn1–N5	96.9 (4)	N3–Mn1–N2	83.1 (4)
O3–Mn1–N5	93.1 (3)	O2–Mn1–N4	89.9 (4)
N3–Mn1–N5	83.5 (4)	O3–Mn1–N4	95.3 (3)
N2–Mn1–N5	87.2 (4)	N3–Mn1–N4	89.0 (4)
N4–Mn1–N5	168.9 (4)		

Symmetry codes: (i) $-x + 1, -y, -z + 1$.

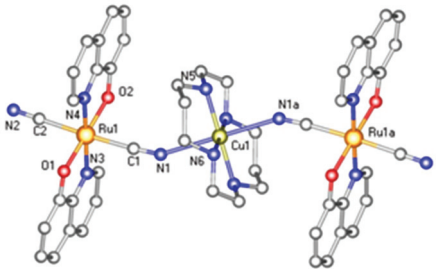

Fig. 7 The perspective view of **5** (symmetry code: (a) $-x + 1, -y, -z$).

Table 5 Selected bond lengths (Å) and angles (°) for **5**

C1–N1	1.145 (9)	Cu1–N5	2.037 (7)
C1–Ru1	2.078 (7)	N3–Ru1	2.098 (9)
C2–Ru1	2.086 (8)	N4–Ru1	2.053 (8)
Cu1–N6	2.012 (7)	O1–Ru1	1.992 (7)
Cu1–N1	2.5094(1)	O2–Ru1	2.021 (6)
N1–C1–Ru1	175.7 (7)	O2–Ru1–C2	88.7 (3)
N2–C2–Ru1	177.5 (8)	N4–Ru1–C2	90.1 (3)
O1–Ru1–O2	179.3 (3)	C1–Ru1–C2	176.8 (3)
O1–Ru1–N4	97.7 (3)	O1–Ru1–N3	80.7 (3)
O2–Ru1–N4	81.6 (3)	O2–Ru1–N3	100.0 (3)
O1–Ru1–C1	92.0 (3)	N4–Ru1–N3	178.4 (3)
O2–Ru1–C1	88.1 (3)	C1–Ru1–N3	90.6 (3)
N4–Ru1–C1	89.4 (3)	C2–Ru1–N3	89.9 (3)
O1–Ru1–C2	91.2 (3)	Cu1–N1–C1	151.55(1)

5.344 Å and the closest interchain Ru···Ru distance is 7.88 Å (Fig. S1†). In contrast to **2** and **3**, there is no π–π interaction between the quinolinolato rings due to the bulkiness of L^1, which prevents effective stacking of the quinolinolato rings.

Reaction of **1** with $[Cu^{II}(cyclam)Br_2]$ in methanol afforded compound **5** which is shown to be a trinuclear molecule by X-ray diffraction analysis (Fig. 7). Selected bond lengths (Å) and bond angles (°) are listed in Table 5. The compound crystallizes in a $P2_1/n$ space group with an inversion centre at the central Cu^{II} ion. The Ru–C (2.078 and 2.086 Å) bond lengths and Ru–C–N bond angles (175.7(7) and 177.5(8)°) are essentially identical to those of **1**. The Cu^{II} atom has a Jahn–Teller distorted octahedral geometry, with the equatorial Cu–N bond distances (2.012(7)–2.037(7) Å) much shorter than the axial ones (2.5094(1) Å). The adjacent Ru···Cu distance is 5.53 Å and the Ru···Ru intramolecular distance is 11.05 Å. The packing diagram of **5** (Fig. S2†) shows extensive π–π stacking interactions among the quinolinolato rings, leading to an extended supramolecular network.

Reaction of **1** with $[Ni^{II}(cyclam)Cl_2]$ in methanol afforded the trinuclear compound **6**. The IR spectrum shows a $\nu(C{\equiv}N)$ stretching band at 2106 cm^{-1}. X-ray crystallography shows a Ru–Ni–Ru arrangement for **6** (Fig. 8), which is isostructural to that of **5**. Selected bond lengths (Å) and bond angles (°) are listed in Table 6. Compound **6** crystallizes in a $P2_1/n$ space group with an inversion center passing through the Ni^{II} centre. The structure is also similar to the trinuclear complex {Ni(-cyclam)[Ru(acac)$_2$(CN)$_2$]$_2$}.[14] The intramolecular Ru···Ni distance is 5.29 Å and the closest intermolecular Ru···Ru separation is 8.94 Å. As in **5**, there are extensive face-to-face π–π

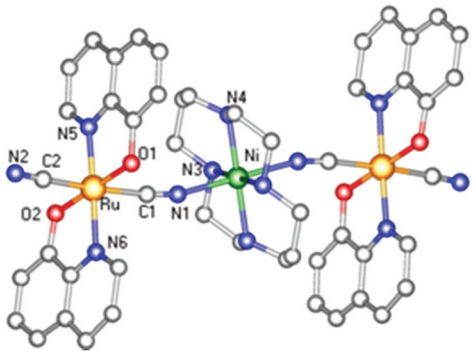

Fig. 8 The perspective view of **6**.

Table 6 Selected geometric parameters (Å, °) for **6**

Ru–O2	1.994 (6)	Ru–N6	2.123 (7)
Ru–O1	2.008 (5)	Ru–C1	2.095 (5)
Ru–N5	2.050 (7)	Ni–N3	2.078 (4)
Ru–C2	2.060 (5)	Ni–N4^{i}	2.093 (3)
O2–Ru–O1	179.5 (2)	N3–Ni–N4^{i}	94.15 (15)
O2–Ru–N5	97.0 (3)	N3–Ni–N4	85.85 (15)
O1–Ru–N5	83.4 (3)	N3–Ni–N1^{i}	91.38 (15)
O2–Ru–C2	90.5 (2)	N3–Ni–N1	88.62 (15)
O1–Ru–C2	89.6 (2)	N4^{i}–Ni–N1	89.36 (13)
N5–Ru–C2	90.2 (2)	N4–Ni–N1	90.64 (13)
O1–Ru–C1	86.47 (19)	C2–Ru–N6	89.3 (2)
N5–Ru–C1	88.1 (2)	C1–Ru–N6	92.6 (2)
C2–Ru–C1	175.85 (18)	N5–Ru–N6	177.9 (3)
O1–Ru–N6	98.6 (3)		

Symmetry codes: (i) $-x + 1, -y + 1, -z + 1$.

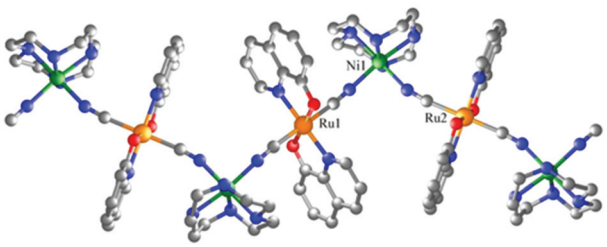

Fig. 9 The 1-D *zigzag* chain constructed by alternating Ru^{III}–Ni^{II} units.

stacking interactions between the quinolinolato rings with the centroid-to-centroid distance of 3.776 Å (Fig. S3†).

Reaction of **1** with $[Ni^{II}(cyclen)Cl_2]$ in methanol produced the block crystals $\{[Ru^{III}(Q)_2(CN_2)][Ni(cyclen)]\}_n$-$[Ru^{III}(Q)_2(CN_2)]_n$ (**7**). The IR spectrum shows the ν(C≡N) stretches at 2126 and 2098 cm^{-1}, which are assigned to bridging and terminal cyanide, respectively. The X-ray structure of **7** is shown in Fig. 9. Selected bond lengths (Å) and bond angles (°) are listed in Table 7. It consists of 1-D *zigzag* cationic chains consisting of alternating $[Ru(Q)_2(CN)_2]^-$ and $[Ni(cyclen)]^{2+}$ units and the chains are further separated by discrete $[Ru(Q)_2(CN)_2]^-$ units acting as counter ions. The bond lengths of Ni–N_{cyclen} (2.086–2.129 Å) are slightly longer than those of Ni–N_{CN} (2.053, 2.057 Å). The N_{CN}–Ni–N_{CN} bond angle is 88.14°, close to a right angle.

Table 7 Selected geometric parameters (Å, °) for **7**

Ru1–O1	2.015 (5)	Ni–N2	2.054 (5)
Ru1–C1	2.067 (5)	Ni–N1	2.057 (4)
Ru1–N7	2.079 (7)	Ni–N4	2.087 (4)
Ru2–O2	2.005 (4)	Ni–N6	2.099 (4)
Ru2–C2	2.053 (5)	Ni–N3	2.128 (5)
Ru2–N8	2.055 (4)	Ni–N5	2.129 (4)
O1–Ru1–C1	86.8 (2)	C1–Ru1–N7	88.0 (2)
O1–Ru1–C1^{i}	93.2 (2)	C1^{i}–Ru1–N7	92.0 (2)
O1–Ru1–N7	80.7 (2)	O1–Ru1–N7^{i}	99.3 (2)

Symmetry codes: (i) $-x + 2, -y + 2, -z$; (ii) $-x + 1, -y + 1, -z$.

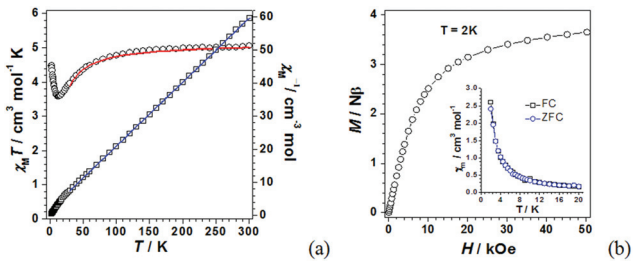

Fig. 10 (a) Temperature dependence of χ_M^{-1} (□) and $\chi_M T$ (○) *vs.* *T* for **2** measured at 1 kOe. (b) Magnetization of **2** as a function of applied field at 2.0 K (inset: plots of ZFC and FC magnetization at 20 Oe).

Magnetic properties

Magnetic measurements were carried out on crystalline samples of compounds **2–7**. The magnetic data show the presence of antiferromagnetic coupling between Ru^{III} and $Mn^{III/II}$ or Cu^{II} spin carriers and ferromagnetic coupling between Ru^{III} and Ni^{II} across the cyanide bridges in compounds **2–7**. Since the cyanide induces a strong crystal field, all mononuclear cyanometallates are at the low-spin state. In systems with octahedral geometry, the single electrons are described by t_{2g} orbitals for the metal ions (M) linked to the carbon end of the cyanide (Ru^{III} in the present case). For the metal ions (M′) linked to the nitrogen, a high spin state occurs in most cases. The nature of the magnetic coupling between M and M′ depends on the electronic configuration of M′. When M′ is Ni^{2+} or Cu^{2+}, ferromagnetic interaction will occur because of the orthogonality of the magnetic orbitals. When M′ is V^{2+}, V^{3+}, or V^{4+}, antiferromagnetic interaction will occur because of the overlap between the magnetic orbitals. However, in the case of high-spin Cr^{2+} (d^4), Mn^{3+} (d^4), Mn^{2+} (d^5), Fe^{2+} (d^6) and Co^{2+} (d^7), the overall exchange interaction is the result of the antiferromagnetic contribution coming from the t_{2g}–t_{2g} overlap and the ferromagnetic one resulting from the orthogonality of the t_{2g}–e_g orbitals. On the basis of above analysis, the magnetic interactions of all the complexes except **5** in this paper agree well with Kahn's orbital symmetry model.[21] The inconsistency of **5** will be discussed below.

Compound 2. The temperature dependence of the molar magnetic susceptibility of **2** was measured in the range of 2–300 K under the external magnetic field of 1 kOe (Fig. 10a). The $\chi_M T$ value at room temperature is 5.05 $cm^3\ mol^{-1}$ K, which

is close to the uncoupled, spin-only value of 5.12 cm^3 mol^{-1} K for one high-spin Mn^{II} center with S = 5/2 and two low-spin Ru^{III} centers with S = 1/2. On lowering the temperature, the $\chi_M T$ value decreases gradually and reaches a minimum value of 3.57 cm^3 mol^{-1} K at ~12 K, and then increases abruptly to reach a value of 4.49 cm^3 mol^{-1} K at 2 K. The molar magnetic susceptibility above 30 K can be fitted by the *Curie–Weiss* law with the *Curie* constant C = 5.18 cm^3 mol^{-1} K and the *Weiss* constant θ = −8.82 K. The negative θ value suggests the presence of antiferromagnetic interaction between neighbouring Ru^{III} and Mn^{II} ions in **2**. The magnetization of this compound as a function of applied field at 2 K is depicted in Fig. 10b. At 50 kOe, the magnetization per $[Mn^{II}Ru^{III}_2]$ reaches a value of 3.64$N\beta$, which is quite different from the expected value of 7.0$N\beta$ for the sum of two Ru^{III} and one Mn^{II} magnetic moments ($S_T = 2S_{Ru} + S_{Mn} = 7/2$; $M_S = gS_TN\beta$), but is close to the value of 3.0$N\beta$ for $S_T = S_{Mn} - 2S_{Ru} = 3/2$, again suggesting that the coupling between Ru^{III} and Mn^{II} ions in **2** is antiferromagnetic. These features are expected for a ferrimagnetic behaviour; the noncompensation of antiferromagnetic coupling between the Ru^{III} spin doublet (t_{2g}^5) and the Mn^{II} spin sextet ($t_{2g}^3e_g^2$) across the cyanide bridge in compound **2** accounts for this well-documented magnetic behaviour. A slight divergence occurs around 2 K in the ZFC/FC plots (Fig. 10b, inset), indicating that long-range ordering may occur below 2 K.[14,22] In contrast, the cobalt analogue $\{[Ru^{III}(Q)_2(CN)]_2(\mu\text{-}CN)_2[Co^{II}(MeOH)_4]\}$ shows 3-D long range ordering at 4.5 K.[15] The weaker magnetic interaction in **2** than in its cobalt analogue is probably the reason why ferromagnetic-like behaviour is not observed in this compound.

On the basis of the crystal data of **2**, we can assume that magnetic interaction between Ru ions can be neglected due to their large separation. Thus, in order to evaluate the value of the magnetic exchange interaction between Ru^{III} and Mn^{II} centres through the cyano bridges in the trimer, the magnetic data were treated by least-squares fitting with the Levenberg–Marquardt algorithm using the program MAGPACK.[23] The best fitted parameters in the temperature range of 20–300 K are J = −4.31 cm^{-1}, g = 2.00, and $R = 9.05 \times 10^{-4}$ [$R = [\Sigma(\chi_{obs} - \chi_{calc})^2/\Sigma(\chi_{obs})^2]$], where J is the coupling constant through the cyano bridges. The antiferromagnetic (AF) coupling between Ru^{III} and Mn^{II} is remarkably larger than that observed in the cyano-bridged trimer Mn^{II}–Fe^{III}–Mn^{II} (J_{Fe-Mn} = −0.44 cm^{-1})[24] and in the compound $\{Mn(CH_3OH)_4[Ru(Salen)(CN)_2]_2\}\cdot 6CH_3OH\cdot 2H_2O$ (J_{Ru-Mn} = −1.8 cm^{-1}).[14]

Compound 3. The temperature dependence of $\chi_M T$ for **3** is shown in Fig. 11a (χ_M is the magnetic susceptibility per $[Ru^{III}Mn^{II}]$ unit). The $\chi_M T$ value at 298 K is 4.76 cm^3 mol^{-1} K, which is close to the uncoupled, spin-only value of 4.75 cm^3 mol^{-1} K for one high-spin d^5 Mn^{II} centre with S = 5/2 and one low-spin d^5 Ru^{III} centre in an octahedral environment with S = 1/2. On lowering the temperature, the $\chi_M T$ value decreases smoothly and attains a minimum value of 3.90 cm^3 mol^{-1} K at 35 K. Upon further cooling, the $\chi_M T$ value increases abruptly and reaches a maximum value of 5.68 cm^3 mol^{-1} K at 6.0 K, consistent with the noncompensation of the spins, resulting

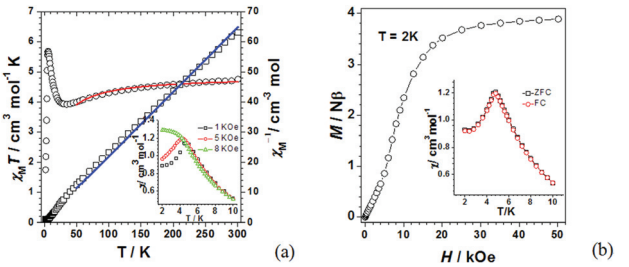

Fig. 11 (a) Temperature dependence of $\chi_M T$ (○) and χ^{-1} (□) for compound **3** (inset: temperature dependence of χ measured in an applied field at 1 kOe (black), 5 kOe (red) and 8 kOe (green) of **3**). (b) Field dependence of the magnetization of **3** (inset: zero-field and field cooled magnetization (ZFCM/FCM) at 20 Oe).

in a ferrimagnetic behavior along the chain with a repeating unit S = 2. Below 6.0 K the $\chi_M T$ value decreases sharply again and reaches a value of 1.75 cm^3 mol^{-1} K at 2 K, which is attributed to field saturation of the magnetization and/or the magnetic anisotropy of the Ru^{III} centres. The χ_M values above 50 K obey the *Curie–Weiss* law [$\chi_M = C/(T - \theta)$] with *Curie* constant C = 4.80 cm^3 mol^{-1} K and *Weiss* constant θ = −11.99 K. At T > 30 K, the decrease of the $\chi_M T$ value and the negative θ value suggest antiferromagnetic (AF) coupling between Ru^{III} and Mn^{II} through the cyano bridges.

It is interesting to note that the sudden decrease of $\chi_M T$ around 6.0 K in **3** is due to the onset of a 3-D antiferromagnetic ordering. Correspondingly, a peak in the χ_M *vs.* T plot at 4.8 K for H = 1 kOe is observed, revealing the occurrence of a weak antiferromagnetic interaction between the bimetallic chains in **3**. The temperature dependent of the zero-field-cooled magnetization and the field-cooled magnetization (ZFCM and FCM) measured in a low field of 20 Oe do not show any divergence. As expected, the ZFCM/FCM plot exhibits a sharp peak at around 4.8 K (Fig. 11b, inset). This 3-D antiferromagnetic ordering is further confirmed by the temperature dependence susceptibility measurements at H_{dc} = 0 Oe and H_{ac} = 3 Oe. The real part (χ_{ac}') of the ac magnetic susceptibility has a maximum at about 4.8 K for frequencies of 10, 100 and 1000 Hz, consistent with the temperature dependency data of dc susceptibility; and the imaginary part (χ_{ac}'') is negligibly small, also suggesting antiferromagnetic ordering below T_N = 4.8 K.

Metamagnetic behaviour was also observed in **3**. The field-dependent magnetization at 2.0 K shows a sigmoidal shape, characteristic of metamagnetic behaviour (Fig. 11b); the magnetization first increases slowly with the external field and then increases sharply, showing a phase transition from antiferromagnetic interaction to a ferromagnetic state. When the field is increased further, the magnetization reaches a value of 3.89$N\beta$ at 50 kOe, close to the value 4.0$N\beta$ expected for an antiferromagnetic coupled $[Ru^{III}Mn^{II}]$ unit with $S_T = S_{Mn} - S_{Ru}$ = 2. The low-temperature magnetic phenomena (T < 10 K) for **3** were further scrutinized by applying various magnetic fields (Fig. 11a, inset). A peak in the χ_M *vs.* T plot is observed at 1 kOe and 5 kOe, which disappears at 8 kOe. The critical field

for such a metamagnetic transition is approximately 6.5 kOe at 2 K, which is determined from the derivative of M against H.

To evaluate the value of the exchange constants of **3**, we used an approximate approach similar to that for 1-D, 2-D, and quasi-2D complexes.[25] The cyanide bridges between Mn^{II} and Ru^{III} are regarded equal, since the bridging modes through cyanide are symmetry-related. Therefore, the 1-D chain can be treated as alternating uniform [$Mn^{II}Ru^{III}$] dimers with the exchange constant J and interchain interactions zJ'. For an asymmetrical [$Mn^{II}Ru^{III}$] dinuclear compound with S_{Mn} = 5/2 and S_{Ru} = 1/2, we regard the g tensors as equal. The spin Hamiltonian is given by eqn (1). Thus the molar magnetic susceptibility of the dimer[21] can be expressed as given in eqn (2), and the molar magnetic susceptibility of the dimer is shown in eqn (3). Then the chain magnetic susceptibility is as shown in eqn (4), in which $u = \coth(J_dS_d(S_d + 1)/kT) - kT/J_dS_d(S_d + 1)$. Furthermore, based on the molecular field theory, the fit function can be modified to include the inter-chain coupling as shown in eqn (5), in which J' is the interchain exchange coupling constant and z is the number of the nearest neighbour chains. The best fitting in the temperature range of 50–300 K gives $J = -1.06$ cm^{-1}, $zJ' = -0.03$ cm^{-1}, $g = 2.02$ with $R = 6.96 \times 10^{-4}$ $\{R = \sum[(\chi_MT)_{obs} - (\chi_MT)_{calc}]^2/\sum(\chi_MT)_{obs}^2\}$. The negative value of exchange coupling through the cyanide bridges further suggests antiferromagnetic interaction between Mn^{II} and Ru^{III} centres.

$$H = -2JS_{Mn}S_{Ru} + \beta(S_{Ni}S_{Ni} + S_{Ru}S_{Ru})H \quad (1)$$

$$\chi_d = \frac{Ng^2\beta^2}{kT} \times \frac{10 + 28e^{6J/kT}}{5 + 7e^{6J/kT}} \quad (2)$$

$$\chi_d = \frac{Ng^2\beta^2}{3kT} S_d(S_d + 1) \quad S_d(S_d + 1) = 3 \times \frac{10 + 28e^{6J/kT}}{5 + 7e^{6J/kT}} \quad (3)$$

$$\chi_{chain} = \frac{Ng^2\beta^2}{3kT}\frac{1+u}{1-u}S_d(S_d + 1) = \frac{1+u}{1-u}\chi_d = \frac{Ng^2\beta^2}{3kT}3\frac{10 + 28e^{6J/kT}}{5 + 7e^{6J/kT}}\frac{1+u}{1-u} \quad (4)$$

$$\chi_M = \frac{\chi_{chain}}{1 - (2zJ'/Ng^2\beta^2)\chi_{chain}} \quad (5)$$

Compound 4. The magnetic susceptibility data for **4** are collected at 5 kOe in the 2–300 K range and are plotted in Fig. 12a. The χ_MT value at 300 K is 3.19 cm^3 K mol^{-1}, which is close to the theoretical value of 3.38 cm^3 K mol^{-1} calculated from non-coupled Ru^{III} (S_{Ru} = 1/2) and Mn^{III} (S_{Mn} = 2) spins assuming $g_{Ru} = g_{Mn} = 2.0$. Lowering the temperature causes χ_MT to decrease slowly and it reaches a value of 2.64 cm^3 K mol^{-1} at 20 K. Upon further cooling, χ_MT increases to 2.72 cm^3 K mol^{-1} at 11 K. Below the peak temperature, χ_MT undergoes a sharp drop down to 1.11 cm^3 K mol^{-1} at 1.5 K, which may be attributed to zero-field splitting and/or interchain antiferromagnetic interactions. The magnetic data at $T > 25$ K were analysed using the *Curie–Weiss* law [$\chi_M = C/(T - \theta)$], affording *Curie* constant C = 3.28 cm^3 K mol^{-1} and *Weiss* constant θ = −10.75 K. The negative θ value and decrease of χ_MT values

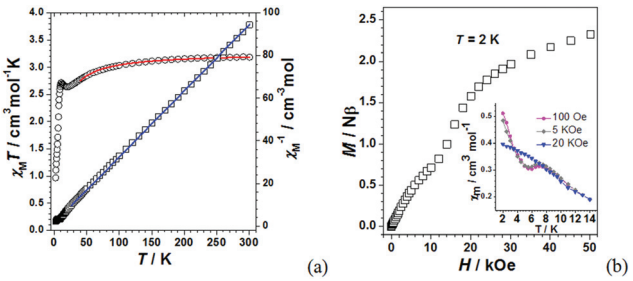

Fig. 12 (a) Temperature dependence of χ_MT (○) and χ_M^{-1} (□) for **4**. (b) Field dependence of the magnetization (inset: temperature dependence of χ measured in an applied field at 100 Oe (pink), 5 kOe (black) and 20 kOe (blue) of **4**).

indicate that antiferromagnetic interactions occur between Ru(III) and Mn(III) *via* cyano bridges in this chain complex.

Zero-field cooled (ZFC) and field-cooled (FC) magnetization experiments performed on **4** in applied fields of 100 Oe do not show any divergence, but they show an obvious inflection point at 7 K, which further indicates a phase transition (Fig. S5†). The further increase of ZFCM/FCM may be attributed to trace paramagnetic impurity. The field-dependent magnetization at 2.0 K shows a sigmoidal shape (Fig. 12b). It first increases slowly with the external field and then increases sharply, showing a phase transition from antiferromagnetic to a ferromagnetic state. When the field is increased further, the magnetization attains a value of 2.32$N\beta$ mol^{-1} (expected value is 3.0$N\beta$ for $S_T = S_{Mn} - S_{Ru}$ = 3/2) at 50 kOe. The low-temperature magnetic phenomena ($T < 15$ K) for **4** were further scrutinized by applying various magnetic fields (Fig. 12b, inset). A peak in χ_M *vs.* T plots is observed at 100 Oe and 5 kOe, and disappears at 20 kOe. The "double-S" shape of the hysteresis loop also supports the occurrence of metamagnetic behaviour (Fig. S6†).

For the nature of Ru^{III} and Mn^{III} interaction, it is expected that when the d_π orbitals on Ru^{III} and Mn^{III} overlap, antiferromagnetic interaction (J_{AF}) will result. On the other hand, the Ru d_π orbitals and Mn d_z^2 orbitals are orthogonal due to π/σ-type symmetry, which is expected to give rise to ferromagnetic interaction (J_F). The orbital overlaps (J_{AF}) would be significantly reduced in the case of the relatively long Mn–N(cyanide) length and acute Mn–N–C(cyanide) angle.[26] The bond lengths of Mn–N(cyanide) in **4** (2.286, 2.302 Å) are comparable with those in [Ru^{III}(salen)$(CN)_2$][Mn^{III}(L)] (2.292(8) and 2.307(8) Å);[20] however, the bond angles of Mn–N–C(cyanide) (154.18° and 149.62°) in **4** are remarkably larger than those of [Ru^{III}-(salen)$(CN)_2$][Mn^{II}(L)] (144.3(8)° and 143.1(8)°). This structural diversity results in completely different magnetic interactions. The structural situation in **4** will render the antiferromagnetic contribution (J_{AF}) larger than the ferromagnetic term (J_F), resulting in net antiferromagnetic coupling in **4**. On the basis of the dimeric model similar to compound **3**, the magnetic susceptibility of the [$Ru^{III}Mn^{III}$] dimer can be expressed by eqn (6), which is derived from the isotropic exchange spin Hamiltonian $H = -2JS_AS_B$. Through the same processing method as compound **3**, the susceptibilities from 40 to 300 K were

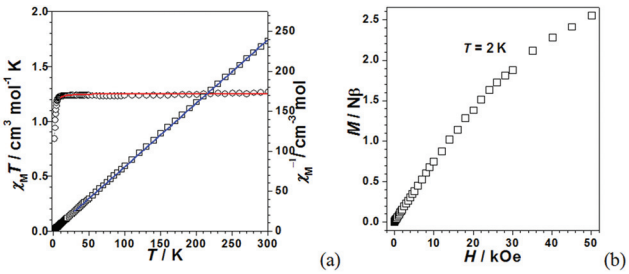

Fig. 13 (a) Temperature dependence of $\chi_M T$ (○) and χ_M^{-1} (□) for **5**. (b) Field dependence of the magnetization of **5** at 2 K.

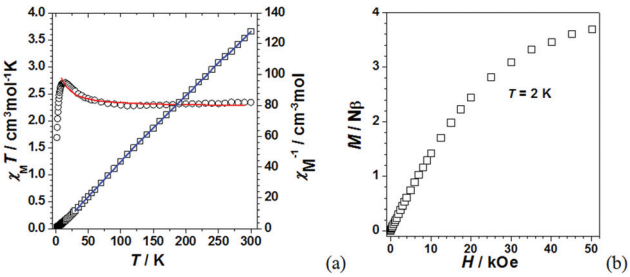

Fig. 14 (a) Temperature dependence of $\chi_M T$ (○) and χ_M^{-1} (□) for **6**. (b) Field dependence of the magnetization of **6** at 2 K.

simulated giving the best fit with parameters $J = -0.75$ cm^{-1}, $zJ' = -0.20$ cm^{-1}, $g = 1.97$ with $R = 7.60 \times 10^{-4}$ $\{R = \sum[(\chi_M T)_{obs} - (\chi_M T)_{calc}]^2/\sum(\chi_M T)_{obs}^2\}$. The negative value of exchange coupling through the cyanide bridges also suggests antiferromagnetic interactions between Mn^{III} and Ru^{III} centers.

$$\chi_d = \frac{Ng^2\beta^2}{4kT} \times \frac{10 + 35e^{5J/kT}}{2 + 3e^{5J/kT}} \quad (6)$$

Compound 5. The magnetic susceptibility data for **5** obey the *Curie–Weiss* law $[\chi_M = C/(T - \theta)]$ at 5 kOe in the 2–300 K range (Fig. 13a). The plot of χ_M^{-1} *vs.* T at $T > 30$ K gives a straight line with *Curie* constant $C = 1.31$ cm^3 K mol^{-1} and *Weiss* constant $\theta = -5.4$ K. The $\chi_M T$ value at 300 K is 1.28 cm^3 K mol^{-1}, which is close to the theoretical value of 1.13 cm^3 K mol^{-1} calculated from two noncoupled Ru^{III} ($S_{Ru} = 1/2$) and a Cu^{II} ($S_{Cu} = 1/2$) spins, assuming $g_{Ru} = g_{Cu} = 2$. The abrupt decrease of $\chi_M T$ below 3 K and the negative value of θ suggest the presence of antiferromagnetic coupling between Ru^{III} and Cu^{II} *via* C≡N bridges in **5**. The magnetization of this compound per $[Cu^{II}Ru^{III}_2]$ unit reaches a value of $2.52N\beta$ mol^{-1} at 2 K and 50 kOe (Fig. 13b), which is slightly smaller than the value of $3.0N\beta$ for the sum of two Ru^{III} and one Cu^{II} magnetic moments ($S_T = 2 \times S_{Ru} + S_{Cu} = 3/2$; $M_s = gS_T N\beta$), suggesting that the antiferromagnetic interaction between the Ru^{III} and Cu^{II} centres is quite weak and the magnetic moments can be aligned in the direction of the applied field when it is large enough at low temperature. On the basis of the trimeric model and through the same processing method as compound **2**, the susceptibilities from 10 to 300 K were simulated giving the best fit with parameters $J = -0.54$ cm^{-1}, $g = 2.11$ with $R = 7.70 \times 10^{-4}$ $\{R = \sum[(\chi_M T)_{obs} - (\chi_M T)_{calc}]^2/\sum(\chi_M T)_{obs}^2\}$. The small negative J value also suggests weak antiferromagnetic coupling of Ru^{III}–Cu^{II}–Ru^{III} *via* bridging cyanides.

According to Kahn's orbital symmetry model,[21] the nature of Cu(II) and Ru(III) interaction should be ferromagnetic (J_F). The observed antiferromagnetic interaction (J_{AF}) of Cu^{II} and Ru^{III} *via* cyano bridges in **5** may be the consequence of the very acute Cu–N≡C angle (151.55(1)°) and long Cu···Ru distance (5.53 Å). A similar antiferromagnetic interaction (J_{AF}) has also been observed in the compound $[Bu_4N][Cu^{II}Ru^{III}(ox)_3]$.[27]

Compound 6. The temperature dependence of $\chi_M T$ for **6** is shown in Fig. 14a. The $\chi_M T$ value at 298 K is equal to 2.34 cm^3 mol^{-1} K, which is larger than the uncoupled, spin-only value of 1.75 cm^3 mol^{-1} K for one high-spin d^8 Ni^{II} center in an octahedral symmetry with $S = 1$ and two low-spin d^5 Ru^{III} centers in an octahedral symmetry with $S = 1/2$. The larger $\chi_M T$ value at room temperature may be due to the significant orbit contribution for both Ni^{II} and Ru^{III} ions in an octahedral environment. The molar magnetic susceptibility of **6** in the temperature range of 20–298 K obeys the *Curie–Weiss* law with *Curie* constant $C = 2.31$ cm^3 mol^{-1} K and *Weiss* constant $\theta = +1.22$ K. The observed *Curie* constant and the positive θ value suggest the presence of ferromagnetic coupling between Ru^{III} and Ni^{II} in **6** through the cyanide bridge. As the temperature is lowered from 298 K, $\chi_M T$ increases smoothly. Below 50 K, $\chi_M T$ increases abruptly, and it reaches a maximum value of 2.70 cm^3 mol^{-1} K at 11 K, further indicating ferromagnetic coupling between Ni^{II} and Ru^{III} centres. Below this peak temperature, $\chi_M T$ undergoes a sharp drop down to 1.69 cm^3 K mol^{-1} at 2 K. The magnetic behaviour of this complex is comparable to a similar compound $\{[Ni^{II}(cyclam)][Ru^{III}(acac)_2(CN)_2]_2\}$.[15] The magnetization measurement was done at the lowest temperature of 2 K and under a high field of 50 kOe in order to reach the saturation value, and to check if the value is close to the expected one. If it was measured at 11 K, the magnetization value would be far from saturation at 50 kOe, although there is ferromagnetic coupling, it will be very weak. The magnetization of this compound per $[Ni^{II}Ru^{III}_2]$ unit reaches a value of $3.68N\beta$ mol^{-1} at 2 K and 50 kOe (Fig. 14b), which is slightly smaller than the value of $4.0N\beta$ for the sum of two Ru^{III} and one Ni^{II} magnetic moments ($S_T = 2 \times S_{Ru} + S_{Ni} = 2$; $M_s = gS_T N\beta$).

In order to evaluate the value of the magnetic exchange interaction between Ru^{III} and Ni^{II} centres through the cyano bridges in the trimer, the magnetic data were treated by least-squares fitting with the Levenberg–Marquardt algorithm using the same program as for compounds **2** and **5**.[22] The best fitted parameters in the temperature range of 10–300 K are $J = 4.85$ cm^{-1}, $g = 2.27$, and $R = 2.50 \times 10^{-4}$ $[R = [\Sigma(\chi_{obs} - \chi_{calc})^2/\Sigma(\chi_{obs})^2]]$, where J is the coupling constant through the cyano bridges. The positive J value suggests ferromagnetic coupling between Ru^{III}–Ni^{II}–Ru^{III} and this value is comparable to that in $\{Ni(cyclam)[Ru(acac)_2(CN)_2]_2\}$.[14]

Compound 7. The temperature dependence of the magnetic susceptibility of **7** measured in the temperature range of 2–300 K under an external magnetic field of 1 kOe is illustrated

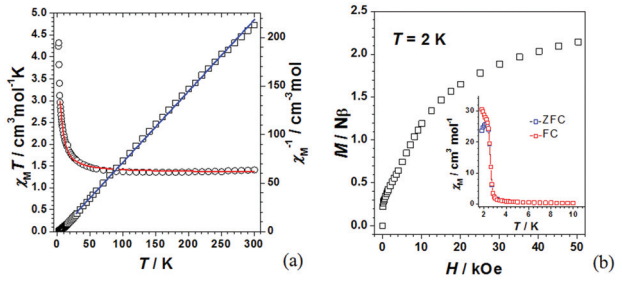

Fig. 15 (a) Temperature dependence of $\chi_M T$ (○) and χ_M^{-1} (□) for **7**. (b) Field dependence of the magnetization of **7** at 2 K (inset: zero-field and field cooled magnetization (ZFCM/FCM) at 20 Oe).

in Fig. 15a. The $\chi_M T$ value at 300 K is equal to 1.41 $cm^3\ mol^{-1}$ K, which is slightly smaller than the uncoupled, spin-only value of 1.75 $cm^3\ mol^{-1}$ K for one high-spin d^8 Ni^{II} center in octahedral symmetry with S = 1 and two low-spin d^5 Ru^{III} centers in octahedral symmetry with S = 1/2. The $\chi_M T$ value begins to increase slowly upon lowering the temperature and reaches 1.47 $cm^3\ mol^{-1}$ K at 50 K. Upon further cooling, the $\chi_M T$ value increases abruptly and reaches a maximum value of 4.32 $cm^3\ mol^{-1}$ K at 2.5 K, which is much larger than the coupled spin-only value of 1.88 $cm^3\ mol^{-1}$ K for S_T = 3/2 resulting from the ferromagnetic coupling of one Ni^{II} (S = 1, g = 2.0) and one low-spin Ru^{III} ion (S = 1/2, g = 2.0). Below 2.5 K, the $\chi_M T$ value decreases and reaches a value of 4.24 $cm^3\ mol^{-1}$ K at 2.0 K. The molar magnetic susceptibility above 30 K could be fitted using the *Curie–Weiss* law [$\chi_M = C/(T - \theta)$], giving a straight line corresponding to *Curie* constant C = 1.38 $cm^3\ mol^{-1}$ and *Weiss* constant θ = +0.61 K. The positive θ value and increase of $\chi_M T$ above 3 K suggest ferromagnetic coupling at high temperature, a result in agreement with Kahn's orbital symmetry model and also in line with previous examples.[15]

To evaluate the value of the exchange constants of **7**, we used the same processing method as compound **3**. The cyanide bridges between Ni^{II} and Ru^{III} were regarded equal, since the bridging modes through cyanide are symmetry-related. Therefore, the 1-D chain can be treated as alternating uniform [$Ni^{II}Ru^{III}$] dimers with the exchange constant J and interchain interactions zj'. For an asymmetrical [$Ni^{II}Ru^{III}$] dinuclear compound with S_{Ni} = 1 and S_{Ru} = 1/2, we regarded the g tensors as equal. The spin Hamiltonian is given by eqn (7). Thus the molar magnetic susceptibility of the dimer[21] can be expressed as given in eqn (8), and the molar magnetic susceptibility of the dimer is also written as in eqn (9). Then the chain magnetic susceptibility is as shown in eqn (10), in which $u = \coth(J_d S_d(S_d + 1)/kT) - kT/J_d S_d(S_d + 1)$. Furthermore, based on the molecular field theory, the fit function can be modified to include the inter-chain coupling as shown in eqn (11), in which J' is the interchain exchange coupling constant and z is the number of the nearest neighbour chains. The best fitting in the temperature range of 50–300 K gives J = 2.38 cm^{-1}, zj' = −0.32 cm^{-1}, g = 2.07 with $R = 2.96 \times 10^{-4}$ $\{R = \sum[(\chi_M T)_{obs} - (\chi_M T)_{calc}]^2/\sum(\chi_M T)_{obs}^2\}$. The positive value of exchange coupling through the cyanide bridges also suggests ferromagnetic interactions between Ni^{II} and Ru^{III} centres.

$$H = -2JS_{Ni}S_{Ru} + \beta(S_{Ni}S_{Ni} + S_{Ru}S_{Ru})H \quad (7)$$

$$\chi_d = \frac{Ng^2\beta^2}{4kT} \times \frac{1 + 10e^{3J/kT}}{1 + 2e^{3J/kT}} \quad (8)$$

$$\chi_d = \frac{Ng^2\beta^2}{3kT} S_d(S_d + 1) \quad S_d(S_d + 1) = 3 \times \frac{1 + 10e^{3J/kT}}{1 + 2e^{3J/kT}} \quad (9)$$

$$\chi_{chain} = \frac{Ng^2\beta^2}{3kT} \frac{1 + u}{1 - u} S_d(S_d + 1) + \frac{Ng^2\beta^2}{3kT} \times S_{Ru}(S_{Ru} + 1) \quad (10)$$

$$\chi_M = \frac{\chi_{chain}}{1 - (2zj''/Ng^2\beta^2)\chi_{chain}} \quad (11)$$

The temperature dependences of the zero-field-cooled magnetization and the field-cooled magnetization (ZFCM and FCM) were measured in a low field of 20 Oe at 1.8–10.0 K. The ZFCM shows a sharp peak at 2.2 K and the FCM increases upon lowering the temperature and diverges with ZFCM at 2.4 K (Fig. 15b, inset). This behaviour is consistent with a spontaneous magnetization under a long range magnetic phase transition. The FO transition is further confirmed by the field dependent isothermal magnetization $M(H)$ performed at 2 K. As shown in Fig. 15b, an abrupt increase of magnetization to a value of *ca.* 0.26 μ_B is observed at 200 Oe. When the external field is further increased, the magnetization shows a slow increase and approaches a value of 2.14 μ_B at 50 kOe, which is smaller than the calculated saturation magnetization (M_s) with a value of 3 μ_B ($S_T = S_{Ni} + S_{Ru}$ = 3/2; $M_s = gS_T N\beta$) for a spin-only system consisting of ferromagnetically coupled Ni^{II} (S = 1) and Ru^{III} (S = 1/2). A hysteresis loop at 2 K (Fig. S7†) was observed with a negligible coercive field, typical of a soft magnet. The presence of 3-D long range magnetic ordering is also evidenced by the ac magnetic data at zero dc and 3 Oe ac field (Fig. 16). Both in-phase and out-of-phase signals, χ_{ac}' and $\chi_{ac}''(T)$,

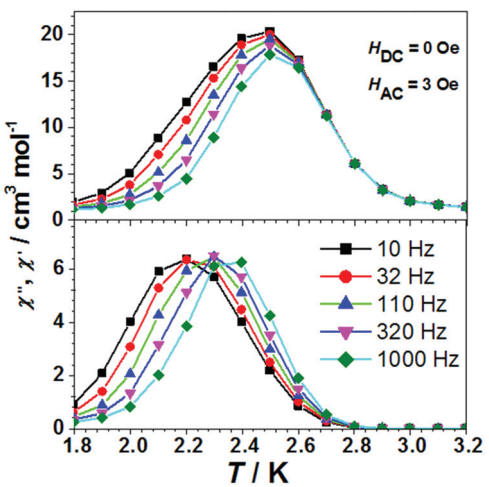

Fig. 16 Temperature dependence of ac susceptibility of **7** measured at zero external magnetic field and H_{ac} = 3 Oe with different frequencies 10 Hz (black), 32 Hz (red), 110 Hz (blue), 320 Hz (pink), and 1000 Hz (green) and in phase χ_{ac}' (upper) and out-of-phase χ_{ac}'' (below).

display a small but non-negligible frequency dependent behaviour, which suggests a slow relaxation process characteristic of a spin glass (SG) transition.[28] The frequency-dependent normalized frequency shift in the freezing temperature, T_f, of the peak temperature shift (ΔT_p) of χ_{ac}', as measured by the parameter $\varphi = \Delta T_p/[T_p \Delta(\log f)] = 0.0041$ (f is the frequency of H_{ac}), is consistent with a glasslike magnetic behaviour. Generally speaking, the φ value is larger than 0.1 for an SMM, while it is usually smaller than 0.01 for a typical SG.[24]

Conclusions

A series of heterobimetallic [$Ru^{III}M$] complexes (M = $Mn^{II/III}$, Cu^{II}, Ni^{II}) have been prepared by the reaction of $[Ru^{III}(Q)_2(CN)_2]^-$ with ML^{n+} (L = ancillary ligand). Antiferromagnetic coupling between the Ru^{III} and $Mn^{II/III}$ has been observed in compounds **2–4**. Moreover, **3** and **4** exhibit metamagnetic behavior with T_N = 4.8 K and 7.0 K, respectively. Antiferromagnetic coupling is also observed between Ru^{III} and Cu^{II} in **5**. On the other hand, ferromagnetic interaction between Ru^{III} and Ni^{II} is found in **6** and **7**. Compound **7** further exhibits long range magnetic ordering below 2.5 K and spin glass behavior. Compared with the polynuclear compounds prepared from other dicyanoruthenium(III) building blocks such as $[Ru^{III}(acac)_2(CN)_2]^-$ or $[Ru^{III}(salen)(CN)_2]^-$, the structures of the compounds reported here are generally of higher dimension as a result of π–π interactions between the quinolinolato ligands. Enhanced magnetic interactions are also observed in these compounds.

Acknowledgements

The work described in this paper was supported by the Hong Kong University Grants Committee Area of Excellence Scheme (AoE/P-03-08) and the NSFC/RGC Joint Research Scheme (N_CityU 107/08) and the National Natural Science Foundation of China (NSFC 20831160505, 21201023 and 21101123).

Notes and references

1 (*a*) L. Öhrström and K. Larsson, *Molecule-Based Materials: The Structural Network Approach*, Elsevier, Amsterdam, 2005; (*b*) M. Krumoo, *Chem. Soc. Rev.*, 2009, **38**, 1353.
2 X.-Y. Wang, C. Avendañoa and K. R. Dunbar, *Chem. Soc. Rev.*, 2011, **40**, 3213–3238.
3 T. D. Harris, M. V. Bennett, R. Clérac and J. R. Long, *J. Am. Chem. Soc.*, 2010, **132**, 3980–3988.
4 J. J. Sokol, A. G. Hee and J. R. Long, *J. Am. Chem. Soc.*, 2002, **124**, 7656–7657.
5 (*a*) E. J. Schelter, J. K. Bera, J. Bacsa, J. R. Galán-Mascarós and K. R. Dunbar, *Inorg. Chem.*, 2003, **42**, 4256–4258; (*b*) E. J. Schelter, A. V. Prosvirin, W. M. Reiff and K. R. Dunbar, *Angew. Chem., Int. Ed.*, 2004, **43**, 4912–4915; (*c*) E. J. Schelter, A. V. Prosvirin and K. R. Dunbar, *J. Am. Chem. Soc.*, 2004, **126**, 15004–15005; (*d*) E. J. Schelter, F. Karadas, C. Avendano, A. V. Prosvirin, W. Wernsdorfer and K. R. Dunbar, *J. Am. Chem. Soc.*, 2007, **129**, 8139–8149; (*e*) K. R. Dunbar, E. J. Schelter, A. V. Palii, S. M. Ostrovsky, V. Y. Mirovitskii, J. M. Hudson, M. A. Omary, S. I. Klokishner and B. S. Tsukerblat, *J. Phys. Chem. A*, 2003, **107**, 11102–11111.
6 M. P. Shores, J. J. Sokol and J. R. Long, *J. Am. Chem. Soc.*, 2002, **124**, 2279–2292.
7 (*a*) A. Müller, W. Eltzner, S. Sarkar, H. Bögge, P. J. Aymonino, N. Mohan, U. Seyer and P. Subramanian, *Z. Anorg. Allg. Chem.*, 1983, **503**, 22–36; (*b*) N. Machida, S. Ohkoshi, Z. J. Zhong and K. Hashimoto, *Chem. Lett.*, 1999, 907–908.
8 D. E. Freedman, D. M. Jenkins and J. R. Long, *Chem. Commun.*, 2009, 4829–4831.
9 (*a*) T. Stawski, J. Szklarzewicz and K. Lewiński, *Transition Met. Chem. (London)*, 2006, **31**, 353–361; (*b*) J. H. Yoon, J. H. Lim, H. C. Kim and C. S. Hong, *Inorg. Chem.*, 2006, **45**, 9613–9615; (*c*) J. H. Yoon, H. C. Kim and C. S. Hong, *Inorg. Chem.*, 2005, **44**, 7714–7716; (*d*) S. W. Choi, D. W. Ryu, J. W. Lee, J. H. Yoon, H. C. Kim, H. Lee, B. K. Cho and C. S. Hong, *Inorg. Chem.*, 2009, **48**, 9066–9068; (*e*) S. W. Choi, H. Y. Kwak, J. H. Yoon, H. C. Kim, E. K. Koh and C. S. Hong, *Inorg. Chem.*, 2008, **47**, 10214–10216; (*f*) J. I. Kim, J. H. Yoon, H. Y. Kwak, E. K. Koh and C. S. Hong, *Eur. J. Inorg. Chem.*, 2008, 2756–2763.
10 (*a*) O. Kahn, J. Larionova and L. Ouahab, *Chem. Commun.*, 1999, 945–952 and references therein; (*b*) J. Larionova, J. Sanchiz, S. Gohlen, L. Ouahab and O. Kahn, *Chem. Commun.*, 1998, 953–954; (*c*) J. Larionova, O. Kahn, S. Gohlen, L. Ouahab and R. Clérac, *J. Am. Chem. Soc.*, 1999, **121**, 3349–3356; (*d*) A. K. Sra, M. Andruh, O. Kahn, S. Golhen, L. Ouahab and J. V. Yakhmi, *Angew. Chem., Int. Ed.*, 1999, **38**, 2606–2609; (*e*) B. Gillon, A. Goujon, S. Willemin, J. Larionova, C. Desplanches, E. Ruiz, G. André, J. A. Stride and C. Guérin, *Inorg. Chem.*, 2007, **46**, 1090–1099; (*f*) J. Larionova, R. Clérac, J. Sanchiz, O. Kahn, S. Golhen and L. Ouahab, *J. Am. Chem. Soc.*, 1998, **120**, 13088–13095; (*g*) J. Larionova, O. Kahn, J. Bartolome, R. Burriel, M. Castro, V. Ksenofontov and P. Gütlich, *Chem. Mater.*, 1999, **11**, 3400–3405; (*h*) J. Larionova, R. Clérac, B. Donnadieu and C. Guérin, *Chem.–Eur. J.*, 2002, **8**, 2712–2716; (*i*) J. Milon, M. C. Daniel, A. Kaiba, P. Guionneau, S. Brandès and J. P. Sutter, *J. Am. Chem. Soc.*, 2007, **129**, 13872–13878.
11 (*a*) M. V. Bennett and J. R. Long, *J. Am. Chem. Soc.*, 2003, **125**, 2394–2395; (*b*) D. E. Freedman, D. M. Jenkins, A. T. Iavarone and J. R. Long, *J. Am. Chem. Soc.*, 2008, **130**, 2884–2885; (*c*) J. M. Zadrozny, D. E. Freedman, D. M. Jenkins, T. D. Harris, A. T. Iavarone, C. Mathonière, R. Clérac and J. R. Long, *Inorg. Chem.*, 2010, **49**, 8886–8896.
12 (*a*) B. Sieklucka, R. Podgajny, P. Przychodzen and T. Korzeniak, *Coord. Chem. Rev.*, 2005, **249**, 2203–2221; (*b*) P. Przychodzeń, T. Korzeniak, R. Podgajny and

B. Sieklucka, *Coord. Chem. Rev.*, 2006, **250**, 2234–2260; (*c*) B. Sieklucka, R. Podgajny, D. Pinkowicz, B. Nowicka, T. Korzeniak, M. Bałanda, T. Wasiutyński, R. Pełka, M. Makarewicz, M. Czapla, M. Rams, B. Gaweł and W. Łasocha, *CrystEngComm*, 2009, **11**, 2032–2039.

13 (*a*) P. M. Kiernan and W. P. Griffith, *J. Chem. Soc., Dalton Trans.*, 1975, 2489–2494; (*b*) T. S. Venkatakrishnan, R. Rajamani, S. Ramasesha and J. P. Sutter, *Inorg. Chem.*, 2007, **46**, 9569–9574; (*c*) R. Pradhan, C. Desplanches, P. Guionneau and J. P. Sutter, *Inorg. Chem.*, 2003, **42**, 6607–6609; (*d*) R. Podgajny, D. Pinkowicz, T. Korzeniak, W. Nitek, M. Rams and B. Sieklucka, *Inorg. Chem.*, 2007, **46**, 10416–10425; (*e*) D. Pinkowicz, R. Podgajny, M. Bałanda, M. Makarewicz, B. Gaweł, W. Łasocha and B. Sieklucka, *Inorg. Chem.*, 2008, **47**, 9745–9747; (*f*) D. Pinkowicz, R. Pełka, O. Drath, W. Nitek, M. Bałanda, A. M. Majcher, G. Poneti and B. Sieklucka, *Inorg. Chem.*, 2010, **49**, 7565–7576; (*g*) M. Arai, W. Kosaka, T. Matsuda and S. Ohkoshi, *Angew. Chem., Int. Ed.*, 2008, **47**, 6885–6887; (*h*) D. Pinkowicz, R. Podgajny, R. Pełka, W. Nitek, M. Bałanda, M. Makarewicz, M. Czapla, J. Żukrowski, C. Kapusta, D. Zając and B. Sieklucka, *Dalton Trans.*, 2009, 7771–7777.

14 (*a*) W.-F. Yeung, W.-L. Man, W.-T. Wong, T.-C. Lau and S. Gao, *Angew. Chem., Int. Ed.*, 2001, **40**, 3031; (*b*) W.-F. Yeung, P.-H. Lau, T.-C. Lau, H.-Y. Wei, H.-L. Sun, S. Gao, Z.-D. Chen and W.-T. Wong, *Inorg. Chem.*, 2005, **44**, 6579; (*c*) W.-F. Yeung, T.-C. Lau, X.-Y. Wang, S. Gao, L. Szeto and W.-T. Wong, *Inorg. Chem.*, 2006, **45**, 6756; (*d*) J.-F. Guo, X.-T. Wang, B.-W. Wang, G.-C. Xu, S. Gao, L. Szeto, W.-T. Wong, W.-Y. Wong and T.-C. Lau, *Chem.–Eur. J.*, 2010, **16**, 3524; (*e*) J.-F. Guo, W.-F. Yeung, P.-H. Lau, X.-T. Wang, S. Gao, W.-T. Wong, S. S.-Y. Chui, C.-M. Che, W.-Y. Wong and T.-C. Lau, *Inorg. Chem.*, 2010, **49**, 1607–1614.

15 J. Xiang, L.-H. Jia, W.-L. Man, K. Qian, S.-M. Yiu, G.-H. Lee, S.-M. Peng, S. Gao and T.-C. Lau, *Chem. Commun.*, 2011, **47**, 8694–8696.

16 A. Altomare, G. Cascarano, C. Giacovazzo, A. Guagliardi, M. Burla, G. Polidori and M. J. Camalli, *Appl. Crystallogr.*, 1994, **27**, 435.

17 P. T. Beurskens, G. Admiraal, G. Beurskens, W. P. Bosman, R. de Gelder, R. Israel and J. M. M. Smits, DIRDIF 99, The DIRDIF-99 program system, Technical Report of the Crystallography Laboratory, University of Nijmegen, The Netherlands, 1999.

18 *Crystal Structure, Single Crystal Structure Analysis Software, version 3.5.1*, Rigaku/MSC Corporation, The Woodlands, Texas, USA, Rigaku, Akishima, Tokyo, Japan, 2003; D. J. Watkin, C. K. Prout, J. R. Carruthers and P. W. Betteridge, *Crystals, Chemical Crystallography*, Lab, Oxford, UK, 1996, issue 10.

19 A. W. Addison, T. N. Rao, J. V. Reedjik and G. C. Verschoor, *J. Chem. Soc., Dalton Trans.*, 1984, 1349–1356.

20 J. H. Yoon, H. S. Yoo, H. C. Kim, S. W. Yoon, B. J. Suh and C. S. Hong, *Inorg. Chem.*, 2009, **48**, 816–818.

21 O. Kahn, *Molecular Magnetism*, VCH, Weinheim, 1993.

22 L. M. Toma, R. Lescouëzec, J. Pasán, C. Ruiz-Pérez, J. Vaissermann, J. Cano, R. Carrasco, W. Wernsdorfer, F. Llore and M. Julve, *J. Am. Chem. Soc.*, 2006, **128**, 4842–4853.

23 J. J. Borrás-Almenar, J. M. Clemente-Juan, E. Coronado and B. S. Tsukerblat, *Inorg. Chem.*, 1999, **38**, 6081–6088.

24 R. Lescouezec, F. Lloret, M. Julve, J. Vaissermann and M. Verdaguer, *Inorg. Chem.*, 2002, **41**, 818–826.

25 (*a*) H.-Z. Kou, B. C. Zhou, S. Gao, D.-Z. Liao and R.-J. Wang, *Inorg. Chem.*, 2003, **42**, 5604–5611; (*b*) B. Chiari, A. Cinti, O. Iovesana and P. F. Zanazzi, *Inorg. Chem.*, 1995, **34**, 2652–2657; (*c*) A. Caneschi, D. Gatteschi, M. C. Melandri, P. Rey and R. Sessoli, *Inorg. Chem.*, 1990, **29**, 4228–4234.

26 H. Miyasaka, A. Saitoh and S. Abe, *Coord. Chem. Rev.*, 2007, **251**, 2622.

27 H. C. Kim, S. W. Yoon, B. J. Suh and C. S. Hong, *Inorg. Chem.*, 2009, **48**, 816–818.

28 (*a*) J. A. Mydosh, *Spin Glasses*, Taylor and Francis, Washington, DC, 1993; (*b*) C. J. O'Connor, *Research Frontiers in Magnetochemistry*, World Scientific, River Edge, NJ, 1993; (*c*) F.-P. Huang, J.-L. Tian, D.-D. Li, G.-J. Chen, W. Gu, S.-P. Yan, X. Liu, D.-Z. Liao and P. Cheng, *Inorg. Chem.*, 2010, **49**, 2525–2529.